Solar Energy 136 (2016) 668–674

Contents lists available at ScienceDirect

Solar Energy

journal homepage: www.elsevier.com/locate/solener

A structurally modified perylene dye for efficient luminescent solar concentrators

Yilin Li, Joseph Olsen, Kenny Nunez-Ortega, Wen-Ji Dong *

School of Chemical Engineering and Bioengineering, Washington State University, Pullman, WA 99164, United States

ARTICLE INFO

Article history:
Received 23 May 2016
Received in revised form 14 July 2016
Accepted 27 July 2016
Available online 2 August 2016

Keywords:
Luminescent solar concentrator
Intramolecular charge transfer
Power conversion efficiency
Cost-effectiveness analysis

ABSTRACT

A structurally modified perylene dye with broad absorption (300–550 nm), long-wavelength emission (550–650 nm), large Stokes shift ($\Delta\lambda$ = 90 nm) and high photoluminescence quantum yield (Φ_f = 0.95) has been synthesized for luminescent solar concentrators (LSCs). Its unique photophysical properties is attributed to the intramolecular charge transfer (ICT) characteristic within the molecule, which was investigated in solution and solid of the dye by spectroscopic measurements as well as theoretical calculations. The performance of LSCs with different device sizes and solar cell configurations was studied experimentally under outdoor real-time sunny condition. Specifically, a LSC with a geometric gain (G) of 5 exhibits high power conversion efficiency (η_{LSC}) of 2.81% ± 0.06% and over unity concentration ratio (C) of 1.19 ± 0.03 with high optical efficiency (P) of 23.7% ± 0.5%. Cost-effectiveness analysis was performed on the LSCs implies that C could be as high as 13.85 (G = 200) and price per watt could be as low as $0.33/W ($G$ = 103).

© 2016 Elsevier Ltd. All rights reserved.

1. Introduction

A luminescent solar concentrator (LSC) generally consists of a planar waveguide doped with luminescent materials and a solar cell attached to one or more edges of the waveguide. Such design is capable of collecting sunlight over a large area, converting it into luminescent light, and concentrating the luminescent light into a small area by the total internal reflection (TIR) mechanism (Weber and Lambe, 1976; Goetzberger and Greube, 1977). Based on this concept, LSC is expected to output a relatively higher power than the attached solar cell under the same sunlight, and meanwhile significantly reduce the use of solar cell materials (Batchelder et al., 1979).

During the development of LSC, numerous efforts have been made in the past decade to either achieve high-efficiency devices or explore practical applications. LSCs doped with colored dyes have reached high power conversion efficiency (PCE) from 4.2% to 7.1% (Desmet et al., 2012; Chou et al., 2015; Goldschmidt et al., 2009; Slooff et al., 2008). Meanwhile experimental studies are extended from small laboratory modules to outdoor building materials (Debije and Rajkumar, 2015; Vossen et al., 2016). Recently, LSCs doped with UV/NIR-harvesting dyes have been reported, which has opened an avenue for light-harvesting smart window technology. These transparent devices are close to regular glass with visible transparency around 85% and exhibit PCE around 0.5% (Zhao and Lunt, 2013; Zhao et al., 2014). There is no doubt that high-efficiency and practical application are two major topics in current LSC research, and thus the role of luminescent materials is of great importance and therefore, developing specific luminescent materials for LSCs is urgent. The ideal luminescent materials for LSCs should have the following photophysical properties: (i) broad absorption that covers the solar spectrum before the band gap of the edge-attached solar cells; (ii) long-wavelength emission centered at the strongest spectral response region of the edge-attached solar cells; (iii) large Stokes shift with minimal spectral overlap that can minimize the self-absorption probability; and (iv) high photoluminescence quantum yield (PLQY) that can achieve a high efficiency for the photon down-shifting process (Hernandez-Noyola et al., 2012). Among all luminescent materials, perylene-based organic dyes have drawn wide attentions because of their high PLQYs and tunable absorption and emission properties via structural modifications (Debije and Verbunt, 2012; Sanguineti et al., 2013). However, due to the planar structures that promote π-π^* electron transition, conventional perylene dyes exhibit two drawbacks relevant to their photophysical properties. One is that the absorption is particularly narrow, which is not capable of covering the short-wavelength (<400 nm) region of solar spectrum. The other is that the Stokes shift is extremely small

* Corresponding author.
E-mail address: wdong@vetmed.wsu.edu (W.-J. Dong).

http://dx.doi.org/10.1016/j.solener.2016.07.051
0038-092X/© 2016 Elsevier Ltd. All rights reserved.

(typically <20 nm), which directly increases the self-absorption probability (Berlman, 1970; Nijegorodov and Downey, 1994). Both features make the conventional perylene dyes non-ideal materials for LSCs.

The most effective and efficient approach to address the two drawbacks of conventional perylene dyes is to change the intrinsic electron transition type, i.e. from π-π* to n-π*, to broaden the absorption and enlarge the Stokes shift, and consequently shift the emission to longer wavelength. It has been reported in the research field of organic photovoltaics that conjugating an electron-deficient group to an electron-rich group introduces n-π* electron transition and the resulting molecules exhibit broad absorption, large Stokes shift and long-wavelength emission (Keerthi et al., 2012; Cremer and Bauerle, 2006; Bell et al., 2005; Weidelener et al., 2012). Our recent studies have proven that these photophysical improvements are attributed to the intermolecular charge transfer (ICT) characteristic within the molecules (Li et al., 2012, 2013a). In addition, ICT-induced energy transfer from the charge donor moiety to charge acceptor moiety within the molecule can also maintain a high PLQY during our extensive studies on organic luminescent molecules for luminescent down-shifting (Li et al., 2013b, 2014, 2015). Therefore, we hypothesized that perylene dyes with ICT characteristic will exhibit n-π* electron transition and the molecules will be more photophysically ideal for LSCs. To test this hypothesis, we designed and synthesized a new perylene dye (dye **1**) based on a perylene structure – 3,9-perylenedicarboxylic acid diisobutyl ester (PDE), which is an electron-deficient structure and has been widely used as a building block for luminescent down-shifting but has not yet been used for LSCs (Jiang et al., 2013). Its conjugation to two electron-rich triphenylamine (TPA) groups leads the resulting dye to exhibit improved photophysical properties for LSCs. The performance of LSCs doped with this dye is superior to R305 dye (a conventional perylene dye) that is used in most LSCs.

2. Results and discussion

2.1. Synthesis of dye *1*

The synthetic route of the proposed perylene dye (dye **1**) is depicted in Scheme 1. In the chemical structure of dye **1**, two electron-rich TPA groups are conjugated to electron-deficient PDE group, thus promoting n-π* electron transition that introduces ICT characteristic (Tang et al., 2010). The synthesis of dye **1** includes two reaction steps. Briefly, PDE (dye **2**) was brominated by N-bromosuccinimide in DMF, which leads to the bromination on the 4- and 10-position of PDE group, and affords dye **3**. Further reaction of dye **3** with 4-(diphenylamino)phenylboronic acid by palladium catalyst through Suzuki cross coupling affords dye **1**, which was then characterized by NMR and MS to verify the structure and purity.

2.2. Photophysical properties of dye *1*

Having successfully synthesized dye **1**, we then prepared solid samples of dye **1** and dye **2** for the comparison on their photophysical properties. The reason for studying the solid samples in poly (methyl methacrylate) (PMMA) matrix rather than the solution samples in typical organic solvents is because the measured photophysical properties such as absorption, emission and PLQY are more related to the actual properties of dye **1** when it is doped in LSCs. The measured spectra are depicted in Fig. 1 and the penitent photophysical parameters are listed in Table 1.

It is noted in Table 1 that despite a unity PLQY (Φ_f = 1.00), dye **2** exhibits photophysical properties that are not favorable for LSCs primarily due to its intrinsic π-π* electron transition, which correlates to the mirror image pattern between its absorption and emission spectra as depicted in Fig. 1a. The narrow absorption (400–500 nm) and short-wavelength emission (450–550 nm) suggest insufficient coverage for solar spectrum and ineffective absorption for solar cells, respectively. Moreover, its small Stokes shift ($\Delta\lambda$ = 17 nm) results in a large spectral overlap that significantly promotes self-absorption. The self-absorption cross section $\left(\sigma_{SA} = \frac{\int \mathrm{Abs}(\lambda)\mathrm{Em}(\lambda)\mathrm{d}\lambda}{\int \mathrm{Em}(\lambda)\mathrm{d}\lambda}\right)$ (Krumer et al., 2013) of dye **2** is calculated at 8.8%, which is relatively higher than other organic dyes that are used in LSCs, such as Rhodamine 6G (8.5%), BASF Lumogen O240 and R305 (conventional perylene dyes, both are 6.7%).

By conjugating with two TPA groups, dye **2** was turned into dye **1**, which exhibits totally different photophysical properties as listed in Table 1. It is noted in Fig. 1b that the mirror image pattern no longer exists in dye **1**, indicating that there is no π-π* electron transition within the molecule. The short-wavelength absorption of TPA (Fig. S1) allows dye **1** to have a broad absorption (300–550 nm). Dye **1** also possesses a large Stokes shift ($\Delta\lambda$ = 90 nm) with a long-wavelength emission (550–650 nm) and high PLQY (Φ_f = 0.95). All these feature are attributed to the n-π* electron transition that introduces the ICT characteristic within the dye **1**. Moreover, σ_{SA} of dye **1** is as low as 4.4%. The unique photophysical properties of dye **1** strongly suggests that dye **1** is a good candidate for LSCs.

2.3. ICT characteristic of dye *1*

To further understand the ICT characteristic within dye **1**, we then conducted spectroscopic measurements and theoretical calculations. It is well-known that ICT induces huge dipole change of the molecule from its ground state to excited state, and such change can be observed by solvatochromism measurement by monitoring the change of Stokes shift (in wavenumber) with solvent orientation polarizability (Δf) (Moss et al., 2010). The ICT-induced energy transfer was studied by time-resolved fluorescence lifetime measurement by comparing the fluorescence lifetime (τ_f) of the solid samples of dye **1** to dye **2**. Furthermore, theoretical cal-

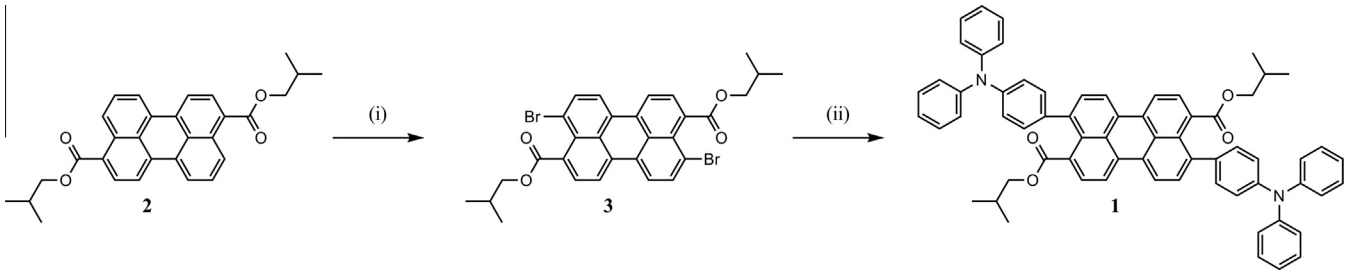

Scheme 1. Synthetic route of dye **1**. Reaction reagents and conditions: (i) N-bromosuccinimide, DMF, 60 °C, 16 h; (ii) 4-(diphenylamino)phenylboronic acid, $Pd(PPh_3)_4$, K_2CO_3 (aq), EtOH, toluene, reflux, 16 h.

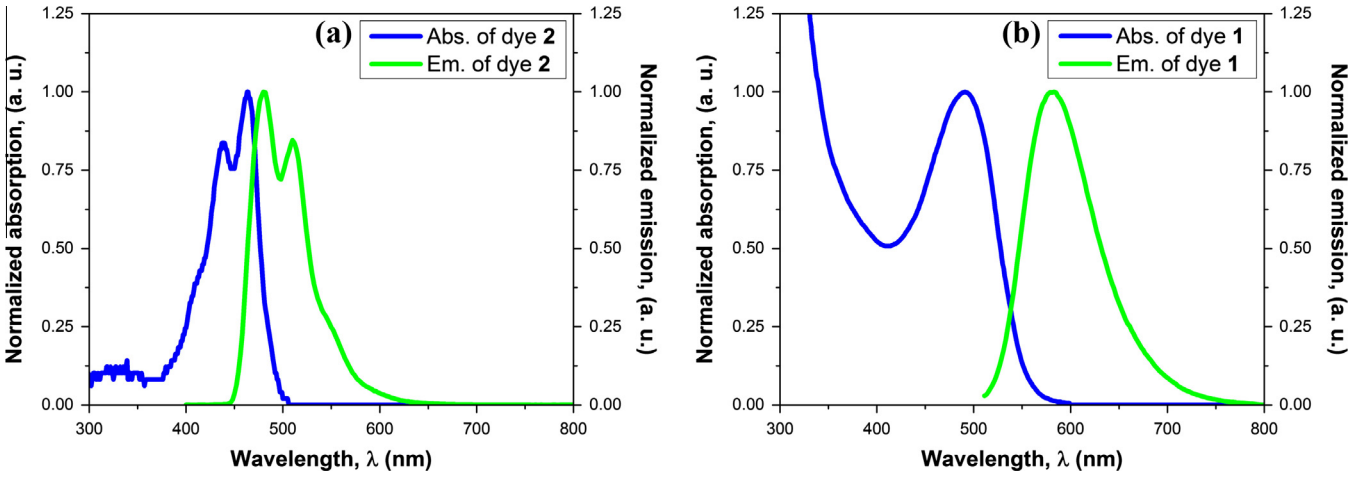

Fig. 1. Normalized absorption and emission spectra for the solid samples of (a) dye **2** and (b) dye **1**.

Table 1
Photophysical parameters including absorption maximum (λ_{abs}), emission maximum (λ_{em}), Stokes shift ($\Delta\lambda = \lambda_{em} - \lambda_{ebs}$), and PLQY ($\Phi_f$) for the solid samples of dye **2** and dye **1**.

Dye	λ_{abs} (nm)	λ_{em} (nm)	$\Delta\lambda$ (nm)	Φ_f[a]
2	463	480	17	1.00
1	491	581	90	0.95

[a] Measured by an integration sphere.

Table 2
Dipole moments (D) of dye **1** and charge distributions (%) on its TPA groups and perylene core at ground and excited states.

	Ground state	Excited state	Difference
Dipole moment	4.2 D	13.9 D	9.7 D
TPA groups	65%	6%	±59%
Perylene core	35%	94%	

culations by density functional theory (DFT) on dye **1** were conducted to support our experimental observations. The results are depicted in Fig. 2 and the relevant calculation results are listed in Table 2.

It is noted in Fig. 2a that the Stokes shift of dye **1** increases as Δf increases. According to the solvent effect theory, the huge change in Stokes shift from 2939 cm^{-1} (85 nm) for the least polar solvent condition ($\Delta f = 0.03$) to 4905 cm^{-1} (158 nm) for the most polar solvent condition ($\Delta f = 0.31$) suggests that there is significant dipole-dipole interaction between solute molecules and its surrounding solvent molecules (Lakowicz, 2006). Table 2 confirms the observations that there is huge dipole change (9.7 D) within dye **1** between its ground state and excited state. The reason for such huge dipole change is directly related to the ICT characteristic of dye **1** that about 59% of charge flows from two TPA groups to PDE group from ground state to excited state. It is noted that such charge flow also induces the energy transfer because the measured fluorescence lifetime of dye **1** (4.77 ns) is similar to dye **2** (4.17 ns) in Fig. 2b, indicating the PDE group of dye **1** is the actual emission center, and such observation is consistent with the charge distribution as depicted in Fig. 2c that at excited state of dye **1**, there is almost no charge left on two TPA groups (6%) while there is significant portion of charge on PDE group (94%).

2.4. Performance of LSCs doped with dye 1

After obtaining the photophysical properties and verifying the ICT characteristic of dye **1**, we then used dye **1** to fabricate LSCs. The schematic presentation of LSC and its working mechanism as well as the configurations of solar cells are illustrated in Fig. 3. We studied the relationship between the device performance and sizes (length, L from 1 to 5 in.) in different configurations (1-cell or 4-cell) under outdoor real-time sunny condition. Before presenting experimental results, we first introduce the definition of some concept terms widely accepted in LSC research. The PCE of LSC

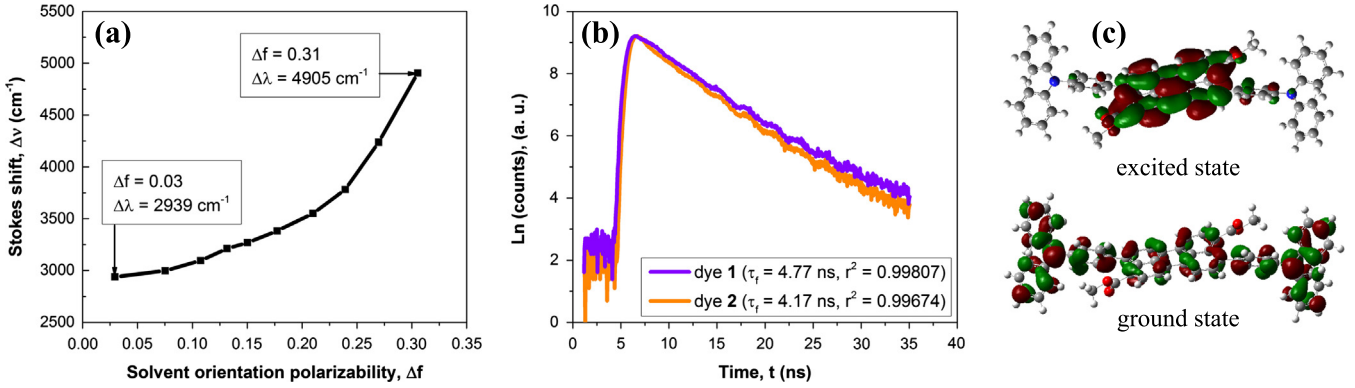

Fig. 2. (a) Change of Stokes shift of dye **1** with Δf; (b) τ_f for the solid samples of dye **1** and dye **2**; and (c) charge distribution of dye **1** at its optimal geometries at ground state and excited state.

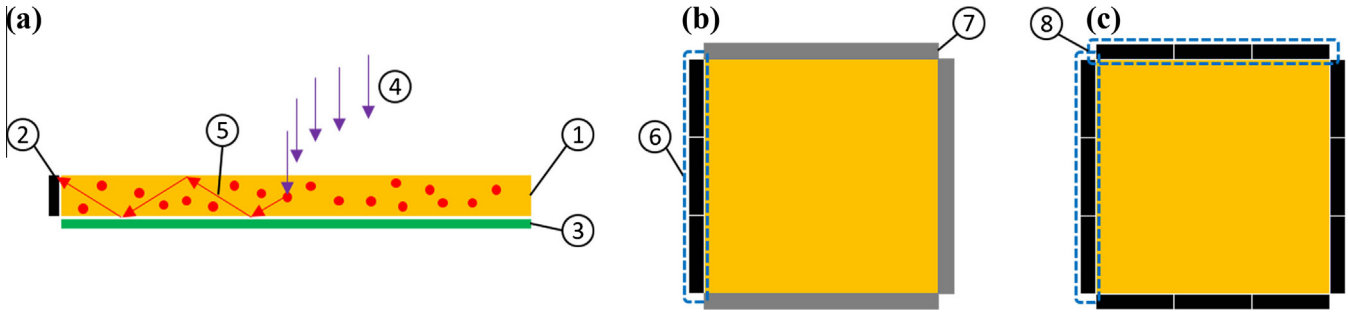

Fig. 3. (a) Side view of schematic presentation of LSC and its working mechanism; and top view of (b) 1-cell and (c) 4-cell configurations of solar cells in a LSC with L = 3. ① Dye doped waveguide, ② edge-attached solar cells, ③ bottom-attached diffuse reflector, ④ sunlight on the top surface, ⑤ luminescent light trapped within the waveguide, ⑥ solar cells on the same edge are connected in series, ⑦ edge-attached mirror reflector and ⑧ solar cells on different edges are connected in parallel.

(η_{LSC}) means how much electrical power is effectively obtained from the device related to the incident power on its top surface. The optical efficiency (P) means the ratio of incident power from the waveguide on the surface of the edge-attached solar cells to incident power on the top surface of the LSC. P and η_{LSC} are linked by the PCE of the solar cell: $\eta_{LSC} = P \times \eta_{cell}$. The geometric gain ($G$) is the ratio of the top surface area of the LSC to the area of the edge-attached solar cells. The concentration ratio (C) is the output power of the LSC to the output power of the edge-attached solar cell under the same incident condition. C and G are linked by P: $C = P \times G$.

The current density-voltage (J-V) curves of the LSCs at various G in 1-cell ($G = 4L$) and 4-cell ($G = L$) configurations are depicted in Fig. 4. The inserts show the relationship of G to η_{LSC} and C. The values of η_{LSC}, C and P at various L for LSCs in 1-cell and 4-cell configurations are listed in Table 3.

It is noted in Fig. 4 that for the J-V curves of LSCs in both 1-cell and 4-cell configurations, there is a decrease trend in short circuit current density (J_{sc}) and an increase trend in open circuit voltage (V_{oc}) as G increases. Such results are due to the experimental setup utilizing small solar cells on each edge of the waveguide connected in series and then connected in parallel if using 4-cell configuration as depicted in Fig. 3c. The larger L is, the more solar cells were used on each edge of the waveguide and thus, increases V_{oc}. For the LSCs with the smallest size ($L = 1$), the huge deviation of J_{sc} observed in Fig. 4 (±0.51 mA cm^{-2} for 1-cell configuration and ±0.94 mA cm^{-2} for 4-cell configuration in Table S1) comes from the light scattering effect of the bottom diffuse reflector, which suggests that the scattered light contributes more J_{sc} than the luminescent materials in small devices (Debije et al., 2009). It is noted in Table 3 that LSCs in 1-cell configuration exhibit higher C (0.42–2.68) than those in 4-cell configuration, which can be attributed to a large G (4–20) that was brought by the edge-attached mirror reflector redirecting the luminescent light to the edge-attached solar cell. However, such configuration increases the photon loss of the devices due to non-perfect total internal reflection and dye self-absorption by increasing the photon transport distance of the luminescent light within the waveguide (Li and Dong, 2015). Therefore, a relatively lower P (10.4–13.4%) and lower η_{LSC} (1.23–1.59%) were observed for LSCs in 1-cell configuration than those in 4-cell configuration (P = 20.6–23.7% and η_{LSC} = 2.44–2.81%). On the contrary, LSCs in 4-cell configuration demonstrate higher η_{LSC} (2.53–2.81%) than those in 1-cell configuration but with relative low C (0.21–1.19). Despite the fact that the highest η_{LSC} (2.81% ± 0.06%) obtained in our experiments is considered relatively low for LSCs doped with single dye (Debije and Verbunt, 2012), which is primarily due to the low efficiency of the solar cell (η_{cell} = 11.8%) used in our experiments, it is noteworthy that the highest P (23.7% ± 0.5%) is superior to that of R305 dye as reported in literature (Desmet et al., 2012). Such high P can lead to a high η_{LSC} of up to 5.8% if high-efficiency III-V GaAs solar cells are used.

2.5. Cost-effectiveness analysis of LSCs doped with dye **1**

Besides the performance of LSCs that was studied on laboratory level, another important evaluation for the practical application of

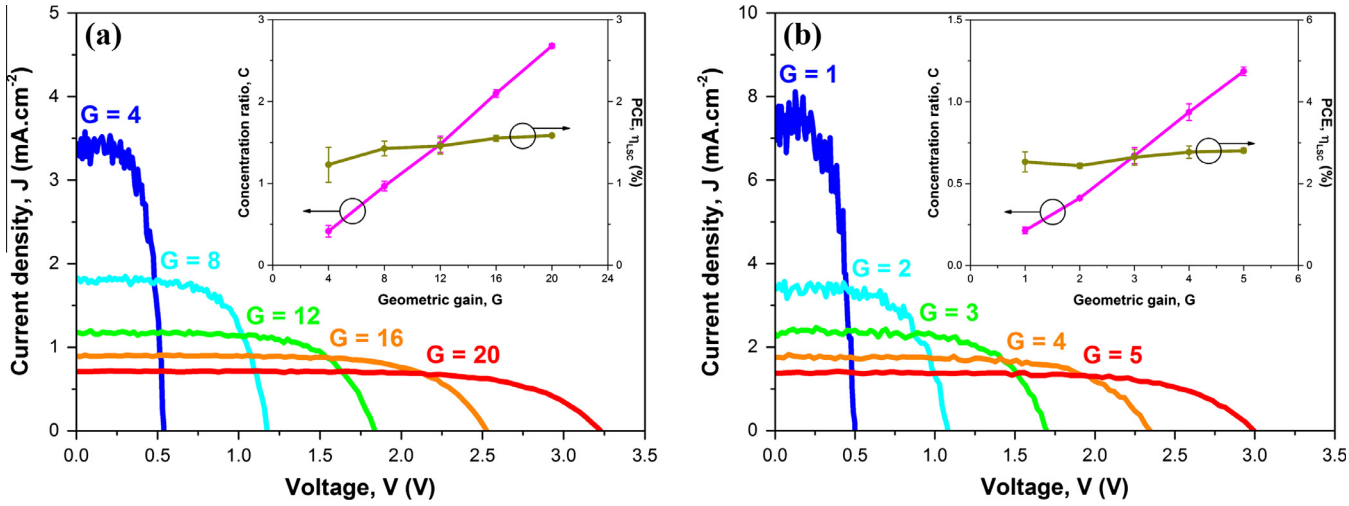

Fig. 4. J-V curves of LSCs in (a) 1-cell and (b) 4-cell configurations as well as the relationship of G to η_{LSC} and C as inserts.

Table 3
Values of η_{LSC}, C and P at various L for LSCs in 1-cell and 4-cell configurations.

L (in.)	1-cell configuration ($G = 4L$)			4-cell configuration ($G = L$)		
	η_{LSC} (%)	C	P (%)	η_{LSC} (%)	C	P (%)
1	1.23 ± 0.21	0.42 ± 0.07	10.4 ± 1.8	2.53 ± 0.25	0.21 ± 0.02	21.4 ± 2.1
2	1.43 ± 0.09	0.97 ± 0.06	12.1 ± 0.8	2.44 ± 0.06	0.41 ± 0.01	20.6 ± 0.5
3	1.46 ± 0.10	1.48 ± 0.10	12.3 ± 0.8	2.65 ± 0.20	0.67 ± 0.05	22.4 ± 1.7
4	1.55 ± 0.03	2.10 ± 0.05	13.1 ± 0.3	2.77 ± 0.15	0.94 ± 0.02	23.4 ± 1.3
5	1.59 ± 0.02	2.68 ± 0.03	13.4 ± 0.1	2.81 ± 0.06	1.19 ± 0.03	23.7 ± 0.5

LSCs is investigating the performance of large-area LSCs, which cannot be done by common laboratory setup. Here, we performed model prediction to investigate the performance as well as the cost-effectiveness of LSCs at large G (10–200), which are depicted in Fig. 5.

It is noted in Fig. 5a that η_{LSC} follows a quasi-exponential decay, decreasing from 1.83% at $G = 10$ to 0.82% at $G = 200$, which suggests an increase in photon loss as G increases. The luminescent light in the center of the waveguide becomes more difficult to transport to the edge-attached solar cells when G increases probably due to the increase of the transportation length of the trapped luminescent light, which raises the probability of surface escaping from both self-absorption-induced light scattering and non-perfect total internal reflection. Further prediction indicates that η_{LSC} starts to be below 0.5% from $G = 617$ (Fig. S2). Although η_{LSC} decreases with G, C increases significantly from 1.55 at $G = 10$ to 13.85 at $G = 200$ as depicted in Fig. 5b, demonstrating a magnitude increase in output power. This further suggests that the power density on the edges of the waveguide is much higher than that of the sunlight. Such increase pattern of C is consistent with other studies when dyes with small spectral overlaps are used (Currie et al., 2008; Gutierrez et al., 2016). In Fig. 5c, the price per watt of LSC decreases sharply at relatively small G (about <100) and increases slowly at relative large G (about >100). Its lowest value is \$0.33/W at $G = 103$ ($\eta_{LSC} = 1.04\%$ and $C = 9.08$), which is only 1/3 of the price per watt of solar cells (assumed at \$1/W). It should be pointed out that the prediction of price per watt of LSC is based on the laboratory cost, which is assumed to be as high as \$10/kg for methylmetharcylate (MMA) polymerization and \$200/g for dye synthesis. We believe that the price per watt of LSC could be as low as \$0.21/W at $G = 170$ (Fig. S3) if the material cost was cut into half when produced in bulk.

3. Conclusion

In this report, we designed and synthesized a new perylene dye – dye **1**, which consists of two electron-rich TPA groups and one electron-deficient PDE group. Because of its intramolecular charge transfer (ICT) characteristic, dye **1** exhibits specific photophysical properties in the solid state, including broad absorption (300–500 nm), red-shifted emission (550–650 nm), large Stokes shift ($\Delta\lambda = 90$ nm) and high PLQY ($\Phi_f = 0.95$). These unique photophysical properties make dye **1** an ideal candidate for LSCs. The performance of LSCs doped with dye **1** was studied under outdoor real-time sunny condition. Specifically, a LSC at $G = 5$ exhibits η_{LSC} as high as 2.81% ± 0.06% and an over unity C at 1.19 ± 0.03 with relative high P of 23.7% ± 0.5%. The model prediction for the large-area LSC implies that C can be achieved as high as 13.85 at $G = 200$ and price per watt can be achieved as low as \$0.33/W at $G = 103$.

4. Experimental

4.1. Dye synthesis and characterization

Reaction (i): *diisobutyl 4,10-dibromoperylene-3,9-dicarboxylate* (dye **3**). In a round-bottom flask, N-bromosuccinimide (4.3 g, 24.3 mmol) was added to a solution of dye **2** (5.0 g, 11.1 mmol) in DMF (100 mL). The reaction mixture was stirred at 60 °C for 16 h. After being cooled down, the reaction mixture was poured into H_2O (400 mL) and filtered. The precipitation was collected and dissolved in DCM (100 mL). The solution was washed by H_2O. The organic layer was collected and dried over anhydrous $MgSO_4$. After filtration, the solvent was removed. The residue was purified by column chromatography on silica, eluting with Hex/DCM (1:3) to afford pure product as orange solid in 50% isolated yield. ^{1}H NMR (300 MHz, $CDCl_3$, δ, ppm): 7.18–7.13 (m, 2H), 7.02–6.94 (m, 4H), 6.78 (d, 2H, J = 8.4 Hz), 4.15 (d, 4H, J = 6.7 Hz), 2.20–2.07 (m, 2H), 1.06 (d, 12H, J = 6.7 Hz). ^{13}C NMR (75 MHz, $CDCl_3$, δ, ppm): 170.1, 170.0, 133.2, 133.1, 131.8, 131.5, 131.3, 131.0, 128.8, 128.6, 128.6, 128.6, 128.5, 128.5, 128.4, 128.3, 121.6, 121.0, 120.4, 119.9, 119.7, 119.4, 72.4, 27.9, 19.7. MALDI-MS: m/z calcd for $C_{30}H_{26}Br_2O_4^+$ 608.0198, found 608.1056.

Reaction (ii): *diisobutyl 4,10-bis(4-(diphenylamino)phenyl)perylene-3,9-dicarboxylate* (dye **1**). In a round-bottom flask equipped with a condenser, dye **3** (300 mg, 0.5 mmol), 4-(diphenylamino) phenylboronic acid (568 mg, 2.0 mmol), $Pd(PPh_3)_4$ (45 mg, 8 mol %) and K_2CO_3 (204 mg, 1.5 mmol, dissolved in 1 mL of H_2O) in a

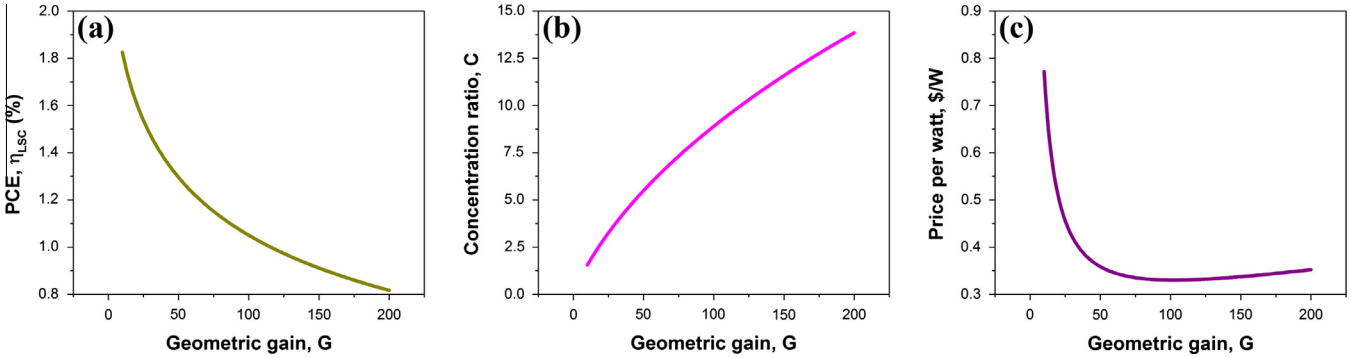

Fig. 5. Relationship of G to (a) η_{LSC}, (b) C and (c) price per watt.

mixture of EtOH (1 mL) and toluene (25 mL) was refluxed for 16 h. After being cooled down, the reaction mixture was extracted by DCM and washed by H_2O. The organic layer was collected and dried over anhydrous $MgSO_4$. After filtration, the solvent was removed. The residue was purified by column chromatography on silica, eluting with Hex/EtOAc (30:1) to afford pure product as dark red solid in 73% isolated yield. ^{1}H NMR (300 MHz, $CDCl_3$, δ, ppm): 8.24–8.14 (m, 4H), 7.12 (d, 2H, J = 7.84 Hz), 7.52 (d, 2H, J = 7.87 Hz), 7.35–7.26 (m, 12H), 7.18–7.13 (m, 12H), 7.06 (t, 4H), 3.57 (d, 4H, J = 6.72 Hz), 1.98–1.85 (m, 2H), 0.93 (d, 12H, J = 6.69 Hz). ^{13}C NMR (75 MHz, $CDCl_3$, δ, ppm): 169.6, 169.5, 147.9, 147.9, 147.2, 147.1, 140.1, 139.3, 137.2, 137.2, 133.9, 133.5, 132.1, 131.3, 131.1, 130.9, 130.0, 129.8, 129.7, 129.6, 129.6, 129.4, 124.7, 123.8, 123.8, 123.3, 122.0, 121.3, 120.7, 119.9, 71.2, 27.9, 19.5. MALDI-MS: m/z calcd for $C_{66}H_{54}N_2O_4^+$ 938.4084, found 938.6151.

4.2. Spectroscopic measurements

Solid samples were prepared by making small waveguides with dimensions of 1 in. × 1 in. × 0.25 in. at low concentration of 10 ppm to avoid any self-absorption issue.

Absorption spectrum was recorded with a Beckman Coulter DU730 Life Science UV-Vis spectrophotometer at room temperature. Emission spectrum was collected on an ISS PC1 photon counting spectrofluorometer at the excitation wavelength of 495 nm at room temperature.

Fluorescence lifetimes were measured on a HORIBA JOBIN YVON fluorocube at room temperature. The excitation wavelength was 495 nm. The fluorescence lifetime data was fitted by a single-exponential equation:

$$I(t) = I_0 \cdot e^{-\frac{t}{\tau_f}}$$

In solvatochromism measurement, the mixtures of 1,4-dioxane (DOX) and acetonitrile (ACN) were used as the solvent. The solvent orientation polarizability (Δf) was calculated by:

$$\Delta f = \frac{\epsilon - 1}{2\epsilon + 1} - \frac{n^2 - 1}{2n^2 + 1}$$
$$\epsilon = \chi_{DOX}\epsilon_{DOX} + \chi_{ACN}\epsilon_{ACN}$$
$$n = \sqrt{\chi_{DOX}n_{DOX}^2 + \chi_{ACN}n_{ACN}^2}$$

where ϵ is the dielectric constant, n is the refractive index of the solvent, and χ is the solvent mole fraction.

4.3. Theoretical calculations

Theoretical calculation was conducted using Gaussian 09 package. Ground state geometry was optimized by using DFT B3LYP/6-31G(d) function. Excited state geometry was optimized by using the time-dependent (TD) method with the same function. The molecular orbitals, dipole moments and charge distributions were then calculated based on the optimal geometries.

4.4. Fabrication and photovoltaic measurement of LSCs

The thickness of the waveguide was 0.25 in. and the dye concentration is 100 ppm. Such selection allows dye **1** (molar absorption coefficient, ε = 28,613 M^{-1} cm^{-1}) to absorb 97% of the sunlight below its direct allowed band gap (2.33 eV or 534 nm, obtained by Tauc relation in Fig. S4). For the preparation of the waveguide, dye **1** (20 mg or 0.01%) and AIBN (radical initiator, 200 mg or 0.1%) was dissolved in MMA (200 g) in an Erlenmeyer flask (500 mL). The solution was stirred in water bath at 85 °C. During the heating, the viscosity of the solution gradually increased. When the viscosity seemed to be higher than that of glycerol, the heating was stopped and the flask was transferred into an ice/water bath at 0 °C. After being cooled down, the solution was poured into a glass mold with dimensions of 8 in. × 8 in. × 0.25 in. The mold was placed in an incubator at 45 °C for 48 h. During this thermal treatment, the syrup turned into a solid slab, which was then transferred to an oven and further cured at 100 °C for 2 h. After being cooled down, the slab can be easily separated from the glass mold. The raw slab was cut and polished into squares to afford waveguides at the length of 1 through 5 in.

The silicon solar cells (1 in. × 0.25 in.) used in the LSC measurement has the following photovoltaic properties: J_{sc} = 29.5 mA cm^{-2}, V_{oc} = 591 mV, FF = 0.68 and η_{cell} = 11.8%. Solar cells were connected in series as a cell unit and then attached to one or more edges of the waveguide by index matching fluid (F-IMF-105, Newport) to obtain LSCs. The bottom of the waveguide was attached with a diffuse reflector (F-16A, White Optics). The performance of LSCs were evaluated in 1-cell and 4-cell configurations. For 1-cell configuration, the other three edges of the waveguide were attached with mirror reflector (Vikuiti, 3M). For 4-cell configuration, the four cell units were connected in parallel. The incident condition was real-time outdoor sunny with power density at 1000 ± 100 W m^{-2}, measured by a solar power meter (SOLAR-100, Amprobe). The *J-V* curves were measured by a sourcemeter (model# 2401, Keithley).

4.5. Model prediction

The model used for prediction is based on our previous report (Li and Dong, 2015). In this model, the self-absorption is described by a coefficient (k), which is related to the G of LSC by a numerical equation obtained from the theories of geometric optics. The absorption and emission spectra of dye **1** in solid state were used in the model. The estimated materials cost – $10/kg for methylmetharcylate (MMA) polymerization and $200/g for dye synthesis, includes reagents, glassware, hardware and utilities in the laboratory.

Appendix A. Supplementary material

Absorption spectrum of solid sample of TPA (Fig. S1). Photovoltaic parameters of the LSCs (Table S1). Predicted η_{LSC} at large G (Fig. S2). Predicted price per watt at reduced material cost (Fig. S3). Calculation of the direct allowed band gap of dye **1** (Fig. S4). ^{1}H NMR, ^{13}C NMR and MALDI-MS spectra of dye **1** and dye **3**. Optimal geometries of dye **1** at ground state and excited state. Supplementary data associated with this article can be found, in the online version, at http://dx.doi.org/10.1016/j.solener.2016.07.051.

References

Batchelder, J.S., Zewail, A.H., Cole, T., 1979. Appl. Opt. 18, 3090–3110.
Bell, T.D.M., Stefan, A., Masuo, S., Vosch, T., Lor, M., Cotlet, M., Hofkens, J., Bernhardt, S., Mullen, K., van der Auweraer, M., Verhoeven, J.W., De Schryver, F.C., 2005. ChemPhysChem 6, 942–948.
Berlman, I.B., 1970. J. Phys. Chem. 74, 3085–3093.
Chou, C.H., Hsu, M.H., Chen, F.C., 2015. Nano Energy 15, 729–736.
Cremer, J., Bauerle, P., 2006. J. Mater. Chem. 16, 874–884.
Currie, M.J., Mapel, J.K., Heidel, T.D., Goffri, S., Baldo, M.A., 2008. Science 321, 226–228.
Debije, M.G., Rajkumar, V.A., 2015. Sol. Energy 122, 334–340.
Debije, M.G., Verbunt, P.P.C., 2012. Adv. Energy Mater. 2, 12–35.
Debije, M.G., Teunissen, J.P., Kastelijn, M.J., Verbunt, P.P.C., Bastiaansen, C.W.M., 2009. Sol. Energy Mater. Sol. C 93, 1345–1350.
Desmet, L., Ras, A.J.M., Boer, D.K.G.d., Debije, M.G., 2012. Opt. Lett. 37, 3087–3089.
Goetzberger, A., Greube, W., 1977. Appl. Phys. 14, 123–139.

Goldschmidt, J.C., Peters, M., Bosch, A., Helmers, H., Dimroth, F., Glunz, S.W., Willeke, G., 2009. Sol. Energy Mater. Sol. C 93, 176–182.
Gutierrez, G.D., Coropceanu, I., Bawendi, M.G., Swager, T.M., 2016. Adv. Mater. 28, 497–501.
Hernandez-Noyola, H., Potterveld, D.H., Holt, R.J., Darling, S.B., 2012. Energy Environ. Sci. 5, 5798–5802.
Jiang, Z., Bogumila, R., Zhang, H., Wang, P., Yamamoto, M., Wang, S., 2013. Patent: US 20130284265 A1.
Keerthi, A., Liu, Y., Wang, Q., Valiyaveettil, S., 2012. Chemistry 18, 11669–11676.
Krumer, Z., Pera, S.J., Dijk-Moes, R.J.A.v., Zhao, Y., Brouwer, A.F.P.d., Groeneveld, E., Sark, W.G.J.H.M.v., Schropp, R.E.I., Donegá, C.d.M., 2013. Sol. Energy Mater. Sol. Cells 111, 57–65.
Lakowicz, J.R., 2006. Principles of Fluorescence Spectroscopy, third ed. Springer Science+Business Media, NY, USA.
Li, Y., Dong, W.-J., 2015. In: 42nd IEEE PVSC.
Li, Y., Scudiero, L., Ren, T., Dong, W.-J., 2012. J. Photochem. Photobiol., A 231, 51–59.
Li, Y., Ren, T., Dong, W.-J., 2013a. J. Photochem. Photobiol., A 251, 1–9.
Li, Y., Li, Z., Wang, Y., Compaan, A., Ren, T., Dong, W.-J., 2013b. Energy Environ. Sci. 6, 2907–2911.
Li, Y., Li, Z., Ablekim, T., Ren, T., Dong, W.-J., 2014. Phys. Chem. Chem. Phys. 16, 26193–26202.
Li, Y., Olsen, J., Dong, W.-J., 2015. Photochem. Photobiol. Sci. 14, 833–841.
Moss, K.C., Bourdakos, K.N., Bhalla, V., Kamtekar, K.T., Bryce, M.R., Fox, M.A., Vaughan, H.L., Dias, F.B., Monkman, A.P., 2010. J. Org. Chem. 75, 6771–6781.
Nijegorodov, N.I., Downey, W.S., 1994. J. Phys. Chem. 98, 5639–5643.
Sanguineti, A., Sassi, M., Turrisi, R., Ruffo, R., Vaccaro, G., Meinardi, F., Beverina, L., 2013. Chem. Commun. 49, 1618–1620.
Slooff, L.H., Bende, E.E., Burgers, A.R., Budel, T., Pravettoni, M., Kenny, R.P., Dunlop, E. D., Buchtemann, A., 2008. Phys. Status Solidi (RRL) 2, 257–259.
Tang, X., Liu, W., Wu, J., Lee, C.S., You, J., Wang, P., 2010. J. Org. Chem. 75, 7273–7278.
Vossen, F.M., Aarts, M.P.J., Debije, M.G., 2016. Energy Build. 113, 123–132.
Weber, W.H., Lambe, J., 1976. Appl. Opt. 15, 2299–2300.
Weidelener, M., Mishra, A., Nattestad, A., Powar, S., Mozer, A.J., Mena-Osteritz, E., Cheng, Y.B., Bach, U., Bauerle, P., 2012. J. Mater. Chem. 22, 7366–7379.
Zhao, Y., Lunt, R.R., 2013. Adv. Energy Mater. 3, 1143–1148.
Zhao, Y., Meek, G.A., Levine, B.G., Lunt, R.R., 2014. Adv. Opt. Mater. 2, 606–611.